Monthly Notices
of the
ROYAL ASTRONOMICAL SOCIETY

MNRAS **534,** 2305–2313 (2024) https://doi.org/10.1093/mnras/stae2186
Advance Access publication 2024 September 20

Impact of environmental conditions on organic matter in astrophysical ice analogues

T. Javelle,[1] A. Ruf,[1,2,3] A. Bouquet,[1] Ph. Schmitt-Kopplin[4,5,6] and G. Danger [1,7]★

[1] *Laboratoire de Physique des Interactions Ioniques et Moléculaires, Institut Origines, Aix-Marseille Université, UMR 7345, CNRS, F-13013 Marseille, France*
[2] *LMU Munich, Faculty of Physics, Schellingstraße 4, D-80799 Munich, Germany*
[3] *Excellence Cluster ORIGINS, Boltzmannstraße 2, D-85748 Garching, Germany*
[4] *Helmholtz Munich, Analytical BioGeoChemistry, Ingolstaedter Landstraße 1, D-85764 Neuherberg, Germany*
[5] *Analytische Lebensmittel Chemie, Technische Universität München, Maximus-von-Forum 2, D-85354 Freising, Germany*
[6] *Max Planck Institute for Extraterrestrial Physics, Gießebachstraße 1, D-85748 Garching bei München, Germany*
[7] *Institut Universitaire de France, IUF, F-75005 Paris, France*

Accepted 2024 September 13. Received 2024 August 29; in original form 2024 February 12

ABSTRACT

The existence of organic matter presenting a high molecular diversity in extraterrestrial environments is well documented. To understand the origin of this organic diversity, laboratory experiments were developed and showed that irradiation and thermal alteration of simple molecules such as methanol, water, and ammonia in conditions mimicking astrophysical ice environments. Ices containing water, methanol, and ammonia (H_2O: MeOH: NH_3) photolyzed and monitored by infrared spectroscopy, while the organic matter formed at room temperature was analyzed *in situ* with infrared spectroscopy and *ex situ* with high-resolution mass spectrometry. Those ices irradiated at 77 K and 10^{-8} mbar shows a significant organic molecular diversity: residual organic compounds contain up to 78 C, 188 H, 123 N, and 37 O. Most of them contains all four CHNO atoms (76–86 per cent), followed by CHO (11–17 per cent), and CHN compounds (5–6 per cent). CHNO and CHO compounds are more aliphatic (34–53 per cent), while CHN compounds are mostly condensed aromatics (83–90 per cent). In this work, our objective is to investigate impacts of environment on this organic molecular diversity by focusing on three parameters: photon dose, pressure, and heating rate during the warming process. Analyses of the residue formed showed that the heating rate and pressure weakly alter the abundance of the final organic material, while the irradiation rate reduced its abundance at high photon doses by a factor of 8. These results give insights on the impact of icy environment conditions in the evolution of astrophysical organic matter.

Key words: astrochemistry – planets and satellites: composition – ultraviolet: planetary systems.

1. INTRODUCTION

Astrophysical ices are observed in various environments, in the icy grains of the interstellar medium (Wooden et al. 2004), in Solar system bodies such as the icy moons of Jupiter or Saturn systems or in comets. In such environments, ices present various compositions (Mumma & Charnley 2011) and are submitted to different physicochemical alterations (Ciaravella et al. 2020), heating histories (Mousis et al. 2016), as well as different irradiation types (Islam et al. 2014). Previous studies suggest that a part of the organic matter observed in carbonaceous chondritic meteorites could have originated from this ice chemistry (Keller et al. 1994; Pizzarello & Shock 2010; Bertaux & Lallement 2017).

These scenarios are corroborated by ice chemistry experiments that showed the possibility to form organic matter presenting similarities with the one observed in certain meteorites (d'Hendecourt & Dartois 2001; Schmitt-Kopplin et al. 2010; Fedoseev et al. 2015). As inferred by laboratory experiments, these ice alterations are known to form a large molecular diversity, whose molecular composition could be dependent on different parameters. In these experiments, ice analogues are formed in conditions relevant to the studied object and are altered with irradiation processes and then heated up to form at room temperature an organic residue. Analyses of this residual organic material showed a high molecular diversity with ten thousands of compounds (Ruf et al. 2019, 2021; Danger et al. 2022) with masses up to 4 kDa (Danger et al. 2013).

Recent studies demonstrated that the reactivity occurring during the UV processing at Lyman a (121 nm) of H_2O: CH_3OH: NH_3 ice is a two-step mechanism. At low temperature (20 or 77 K), UV interaction with ice molecules leads to the formation of various radicals, such as H, OH, CH_3, CH_3O, $^{\bullet}CH_2OH$, NH_2, or $H^{\bullet}CO$, as well as to relatively simple molecules such as CO or CO_2 (Öberg 2016; Layssac et al. 2020; Gutiérrez-Quintanilla et al. 2021). After this irradiation, the ice is warmed up to room temperature, allowing radicals to diffuse inside the ice, providing their recombination and leading to the formation of new and more complex molecules. This process leads to the molecular diversity observed in residue at the end of such an experiment.

★ E-mail: gregoire.danger@univ-amu.fr

Table 1. Summary of the different conditions used to perform experiments. The irradiation time for each sample, ice compositions, irradiation rates with respect to each principal molecules forming the ice (H_2O, MeOH, NH_3), heating rates, pressures of argon added as well as DBE, O/C, and N/C of residues formed at the end of these experiments are reported. TX refers to heating rate experiments, PX to pressure experiments, and IX to irradiation rate experiments.

Name	Irradiation time (h)	H2O (Measured)	NH3 (Mesaured)	MeOH (Measured)	Irradiation rate (photon/MeOH)	T-rate average (K/min) between 77 and 180K	Pressure of argon added (mbar)	# of attributions (ESI +)	# of attributions (ESI -)	DBE (ESI+)	N/C (ESI+)	O/C (ESI+)	DBE (ESI-)	N/C (ESI-)	O/C (ESI-)
TA	68	2.4	1.5	1	72	0.51	0	4 746	2 539	8.3	0.315	0.226	8.398	0.26	0.408
TB	73	2.1	1.4	1	87	4	0	6 576	3 497	8.1	0.346	0.232	7.507	0.291	0.406
TC	68	4.1	1.8	1	214	8.31	0	6 149	3 550	8.3	0.363	0.228	8.073	0.323	0.404
PA	72	1.1	1.4	1	21	1.65	0	8 030	7 359	9.5	0.365	0.241	7.926	0.312	0.381
PB	71	1.6	1.8	1	34	1.74	22.9	7 282	5 440	9.4	0.361	0.239	7.442	0.301	0.385
PC	70	2.2	1.8	1	44	2.88	216.7	9 015	8 512	10.6	0.345	0.25	8.124	0.289	0.358
IA	161	6.3	1.8	1	1 503	2	77.1	3 967	1 159	7.8	0.214	0.237	3.474	0.07	0.299
IB	7	3.3	2	1	66	2	78	3 676	928	9.4	0.241	0.257	3.722	0.137	0.324
IC	1	2.2	1.7	1	7	2	79.3	4 289	2 086	9.1	0.23	0.252	3.369	0.114	0.367

Previous studies showed the influence of the initial ice composition on the final molecular composition of both residual organic material (Fresneau et al. 2017; Gautier et al. 2020; Ruf & Danger 2022) and organic volatiles (Abou Mrad et al. 2017). Comparison between the type of irradiation used for the ice processing showed that only weak differences are observed (Muñoz Caro et al. 2014).

In this work, we investigate the influence of heating rate, pressure, and photon flux. One parameter concerns the first step that is the influence of the UV dose, i.e. the ratio between the carbonaceous source (methanol) and the number of photons, on the molecular composition of organic residues. The other two parameters concerned the warming phase by modifying the heating rate of a photo-processed ice, as well as the residual pressure into the vacuum chamber. Both Fourier-transform infrared spectroscopy (FT-IR) and Fourier-transform ion cyclotron resonance mass spectrometry (FT-ICR-MS) were used to determine the impact of each parameter in residue formation and composition.

2. METHODS

2.1. Residue synthesis

The experimental setup for interstellar ice analogue synthesis is described elsewhere (Nuevo et al. 2007). Briefly, it is composed of a sample holder holding a MgF_2 window into a vacuum chamber (1.10^{-7} mbar). The sample holder can be cooled down to 77 K using liquid nitrogen (provided by Linde). The system is designed to enable simultaneous irradiation using a H_2 discharge lamp (Lyman α, 121 nm, $\sim 10^{14}$ photons cm^{-2} s^{-1}) and formation of the ice from a reservoir containing an in-house gas mixture containing methanol (prepared from Fisher Chemicals, 99.99 per cent), water (purified with a Millipore Direct Q5 system), and ammonia (purchased from Alphagaz™, 99.98 per cent). Detailed sample synthesis condition can be found in Table 1.

Ice irradiation rates were estimated by comparing the FT-IR deposition rate of each species methanol (integration range 1192–1084 cm^{-1}, band strength $1.6 \pm 0.3.10^{-17}$ cm $molecule^{-1}$, and 3612–3003 cm^{-1}, $1.0 \pm 0.2 \times 10^{-16}$ cm $molecule^{-1}$), ammonia (1047–1006 cm^{-1}, $1.8 \pm 0.4 \times 10^{-17}$ cm $molecule^{-1}$, and 3612–3003 cm^{-1}, $2.3 \pm 0.5 \times 10^{-17}$ cm $molecule^{-1}$) and water [3612–3003 cm^{-1}, 2×10^{-16} cm $molecule^{-1}$, values and uncertainties extracted from (Bouilloud et al. 2015)]. The photon flux of the H_2 lamp was measured by actinometry on the methanol ice photolysis giving $3.7 \pm 0.6 \times 10^{14}$ photon cm^{-2} s^{-1} at a 95 per cent uncertainty.

To modify the pressure inside the vacuum chamber during the heating phase, argon (Alphagaz™ 2 argon from Air Liquide, 99.9999 per cent) was added to reach total pressures of 2, 20, or 200 mbar at 77 K with the pumping system closed. When the vacuum chamber is closed without adding argon, the equilibrium pressure is of 10^{-3} mbar after 16 h, while the pressure is of 10^{-7} mbar when the vacuum chamber is dynamically pumped.

The heating rate was fixed to 0.5, 4.0, or 8.0 K min^{-1}, using a heating resistance controlled with a Lake Shore 335 Temperature Controller. All heating rates were measured between 77 and 180 K. Without any control of the heating rate, the heating is not linear (with different shape depending on the amount of argon added) with an average rate of 2.0 ± 0.3 K $mbar^{-1}$ at 95 per cent uncertainty.

2.2. Analyses of samples

Infrared spectroscopy (FT-IR) was used in transmission mode (BRUKER Vector 22 FTIR Spectrometer, 4000–910 cm^{-1}, 400 scans, 2 cm^{-1} resolution) to monitor the composition of the ice and its evolution during its irradiation. It was also used to analyze residue once formed at room temperature. Residues were also analysed with high-resolution mass spectrometry to obtain information on their molecular composition. Residues were recovered from their MgF2 windows using Methanol. The resulting solution was then diluted by a factor of 10.

A APOLLO II electrospray ionization (ESI) coupled to a Fourier transform ion cyclotron resonance mass spectrometer [FT-ICR-MS, Bruker APEX 12 Qe, 12 T already described elsewhere (Schmitt-Kopplin et al. 2010b)] was used to record high-resolution mass spectra from m/z 100 to 1000. Spectra were recorded acquiring 500 scans in the positive mode, while 1000 scans were used in the negative mode. All masses with a higher S/N than 3 and 1 ppm relative intensity threshold to base peak were extracted for formula annotation.

2.3. FT-ICR data analysis

Peak detection and internal calibration were monitored by Bruker Compass DataAnalysis 5.0 SR1. Internal calibration was done according to molecules extracted from the sample and selected according to their molecular plausibility and the presence of isotopologues. Molecular attribution was then done with an in-house software described here (Tziotis et al. 2011) with 0.5 ppm tolerance, 0 to 100 #C, 0–100 #O, and 0 to 16 #N. Thanks to the ultrahigh resolution of the mass analyzer, together with the high dilution of samples and the mild ESI conditions; no clusters, adducts, multiple charged ion, and chemical reaction into the ionization source were occurring and thus detected.

Two extra filtration steps were monitored: (i) C only and (ii) CH compounds were removed such that a proton was removed for all compounds with semi-entire DBE. All data were then analysed using python 3.8.8. Following formulas were used.

Double bound equivalent (DBE) is

$$\mathrm{DBE} = \frac{2\#\mathrm{C} + 2 - \#\mathrm{H} + \#\mathrm{N}}{2}. \qquad (1)$$

Aromaticity equivalent χ_c is defined according to Yassine et al. (2014) as

$$\chi_c = \frac{2\#\mathrm{C} + \#\mathrm{N} - \#\mathrm{H} - 2m\#\mathrm{O}}{\mathrm{DBE} - m\#\mathrm{O}}. \qquad (2)$$

For both equations, #H, #C, #N, #O are the number of hydrogen, carbon, nitrogen, and oxygen, respectively. For χ_c,m is the fraction of oxygen in the residue and is estimated to be 0.5 for similar experiments (Danger et al. 2016). Three classes of compounds are defined: aliphatic ($0 < \chi_c < 2{,}5$), aromatics ($2.5 < \chi_c < 2$, benzene like molecules), and condensed aromatics ($2.7 < \chi_c$, PAH like molecules).

2.4. Contaminations and reproducibility

Blanks were performed to identify possible contaminants coming from solvents or the experimental set-up. Moreover, high-resolution mass annotations and characteristics (such as Absolute mass defect, DBE versus C) were used as filtration steps in order to exclude possible false annotations. Finally, duplicates were used to demonstrate the reproducibility of the residue synthesis and analytical process (Fig. S6).

3. RESULTS AND DISCUSSION

The impact of studied parameters on organic residues from astrophysical ice analogues were characterized with infrared spectroscopy and FT-ICR-MS (Figs 1 and 2). Only selected data were displayed. All spectra can be seen in Fig. 1 and FT-IR band attribution are reported in Table S1.

FT-IR spectra are comparable to ones previously reported for similar experimental conditions (see Fig. 1; Schutte et al. 1993; Muñoz Caro & Schutte 2003; Fresneau et al. 2017). The presence of ν(CH) at wavenumbers lower than 3000 $\mathrm{cm^{-1}}$ indicates an important aliphatic moiety. Hexamethylenetetramine (HMT) is observed with bands at 1375 (k), 1236 and 1005 $\mathrm{cm^{-1}}$ (not represented Fig. 2; Bernstein et al. 1995; Vinogradoff et al. 2012). Polymethyleneimine (PMI) is also present with bands at 1 356 and 1 212 $\mathrm{cm^{-1}}$ (Vinogradoff et al. 2012). On average, the same FT-IR features are observed in all spectra with comparable band ratio. This indicates high similarities in chemical functions.

FT-ICR-MS spectra present a similar asymmetrical Gaussian shape centred around m/z 250 to 300, and intensities are very similar. As previously observed (Danger et al. 2016), for all spectra the CHNO chemical class is the most abundant (average: 91 per cent in ESI+ and 84 per cent in ESI–), while the CHN class represents in average 6 per cent in ESI+ and 3 per cent in ESI–, and the CHO class 3 per cent in ESI+ and 14 per cent in ESI–. The higher abundance of CHN compounds in ESI+ relative to the higher abundance of CHO compounds in ESI– is related to the better ionization of nitrogen chemical function in ESI+ compared to oxygen functions, while it is the opposite in negative mode (Oss et al. 2010; Gioumouxouzis et al. 2015). The distribution of each CHNO, CHO, CHN class follows the same trend in each sample. As observed with FT-IR, HMT (m/z 140.106745 Da) was detected in ESI+, confirming its formation (Danger et al. 2013).

3.1. Impact of the irradiation rate on residue

The impact of the irradiation rate was characterized by increasing the doses 7.4 × 10^0, 6.6 × 10^1, and 1.5 × 10^3 photons/MeOH (IC, IB, and IA respectively, see Table 1) using fixed ice composition, pressure chamber, and heating rate. Therefore, in experiment IC, the gas deposition rate was 300 times faster than for experiment IA. To prevent analytical bias, ices were formed for 0.8, 7.0, and 161 h, respectively, in order to generate the same ice thickness. Residues formed at the end of experiments were analysed with FT-IR and FT-ICR-MS.

Unfortunately, FT-IR spectra could not have been recorded after ice irradiation and its subsequent warming at 300 K due to the low amount of residue formed. FT-ICR-MS spectra have been recorded in ESI+ and ESI– (see Fig. 1c). To analyse those data, ions signal were annotated with their chemical formula thanks to the combined high-mass accuracy and resolution (Table 1). To focus on the nature of the evolution of samples, each spectrum was cleaned, by extracting the major distribution of absolute mass defect (AMD) versus mz plot. Lists of 3600–4300 in ESI+ mode and 900–2100 in ESI– CHON compounds were then further treated (Table 1).

Mass annotations were performed with 0.5 ppm mass accuracy and 550 000 resolution at $m/z = 200$. Then some indicators such as DBE or aromaticity equivalent (χ_c) (equation 2) could be calculated from the elementary compositions to obtain information on molecular structures. For each sample, both ESI+ and ESI– lists were concatenated and this information is displayed in Fig. 3. As usually seen in such astrophysical analogues, compounds containing CHNO atoms are the major chemical group in number (76–86 per cent), followed by CHO compounds (11–17 per cent) and CHN (5–6 per cent). No C only or CH compounds can be seen in ESI. The aromaticity

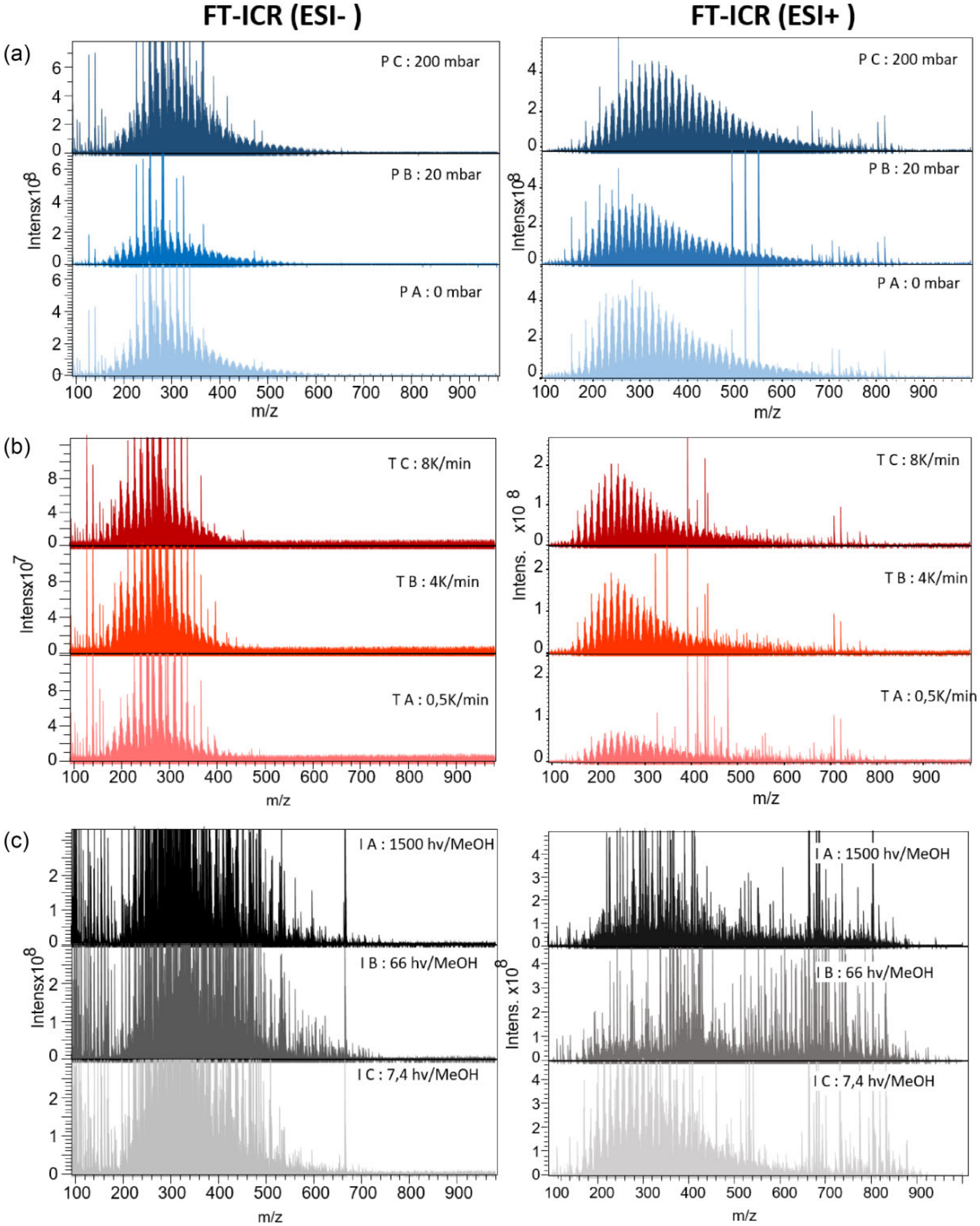

Figure 1. Display of ESI+ and ESI– FT-ICR spectra for global mass range on each different spectral series: (a) the add of global pressure during the heating phase of the irradiated residue (Ref. = 10^{-7} mbar during all heating); (b) the different heating rate during the heating phase (Ref. = 2 K/min); (c) the influence of the irradiation rate (Ref. = 141 photon/MeOH). Extra details can be seen in Fig. S1, Fig. S2, and Fig. S6.

equivalent (χ_c) shows that CHN compounds are mostly condensed aromatics (83–90 per cent), while CHNO and CHO compounds are more aliphatic (34–53 per cent). CHO compounds are more condensed aromatic than CHNO. Regarding the evolution with respect to the irradiation, medium irradiation rate is more aromatic than high and low irradiation rate for both CHN and CHNO compounds, while aliphaticity increases with the irradiation rate for CHO. This evolution of the CHO group can be explained by the time parameter. In this study, the irradiation rate was modified by changing the flux of matter and keeping the same ice thickness. Consequently, the most irradiated sample (IA) was processed 161 times longer at 77 K than the less irradiated one (IC) (Table 1). Because of the sticking rate of

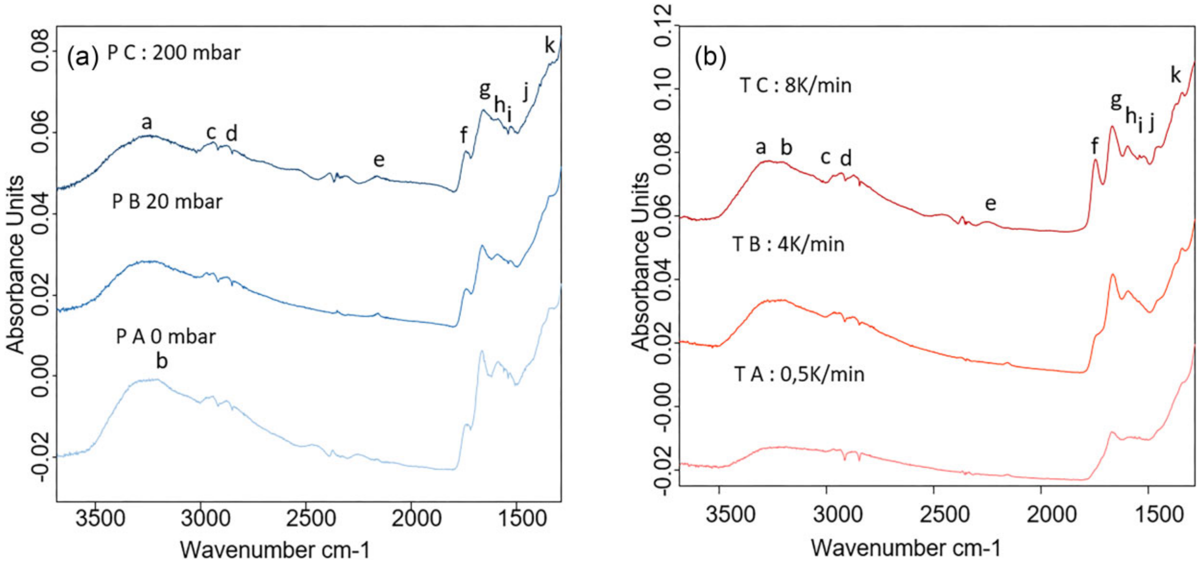

Figure 2. Comparison of FT-IR spectra for each residue at 300 K formed from different conditions (a) pressure variation in the vacuum chamber and (b) heating rate. No IR spectrum could have been recorded for Irradiation series because of a lack of sensitivity. IR bands are marked with attributions and the corresponding assignments are displayed in supplementary material (Table S1).

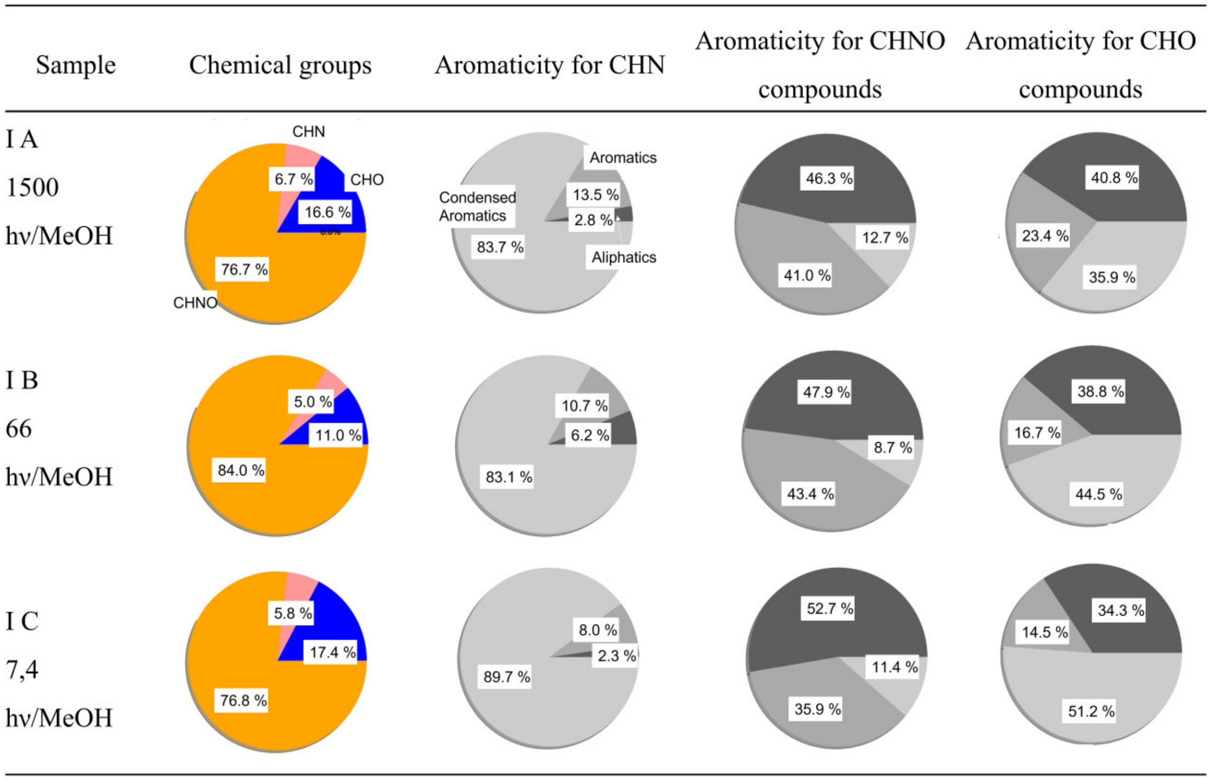

Figure 3. Pie chart representing the percentage of CHNO, CHN, and CHO chemical groups (ESI+ and ESI– modes merged) for 5 Photon/MeOH or 1500 Photon/MeOH. Pie charts for each chemical group are also displayed presenting their relative aromaticity based on the aromaticity equivalent (χ_c) (equation 2). A molecule is defined as aliphatic if $0 < \chi_c < 2.5$, aromatic if $2.5 < \chi_c < 2.7$ (benzene-type molecules) or condensed aromatic if $2.7 < \chi_c$ (PAH-type molecules) (Yassine et al. 2014). CHNO compounds are displayed in orange, CHN in pink, CHO in blue, aliphatic in dark grey, aromatics in grey and condensed aromatics in light grey.

the three different compounds, the H_2O composition of IA was three times higher than IC. Then H_2O could form more $H^\bullet$ radicals, which have more time to diffuse and lead to a reducing organic material compared to other experiments. The impact of irradiation doses in the range used in this work does only slightly influence the nature of the compounds formed in this work.

To obtain additional information about molecules that were the most impacted by the variation of the photon dose, molecules

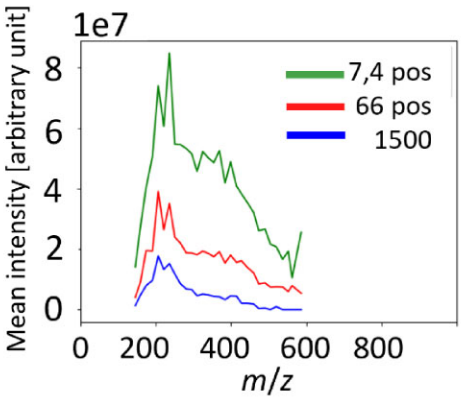

Figure 4. Superimposed mean intensity value (15 Da interval) for decreasing ion mass in ESI+ with respect to the increase of the irradiation rate into the I series with respect to *m/z*. The most 825 (11 per cent of all masses) decreasing masses present in IC, IB, and IA (7.4, 66, and 1.5.10^3 photon/MeOH respectively, see Table 1) were selected with HCE3.5. See Fig. S8 and Fig. S9 for more details.

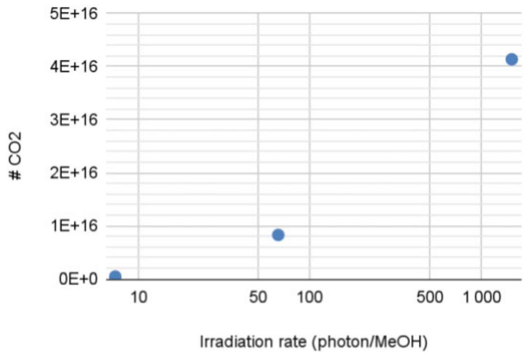

Figure 5. Quantity of CO_2 produced at the end of irradiation process in the irradiation rate series (7.4, 66, and 1.5.10^3 photon/MeOH (IC, IB, and IA respectively, see Table 1) with respect to the irradiation rate. The abscissa axis is in logarithmic scale and log regressions are displayed. The # molecules was calculated from 20 scans IR spectra recorded at 77 K at the end of the irradiation. The band strengths was extracted from Bouilloud et al. (Bouilloud et al. 2015) $A(CO_2, 2350\ cm^{-1}) = 7.6 \times 10^{-17}$ cm molecule^{-1}.

presenting increase or decrease in ESI+ of their intensities during the photon dose variation were extracted and plotted (Fig. 4). Increasing molecules correspond to 2.9 per cent in number of the whole molecules and are randomly displaced along the mass spectrum, H/C versus N/C and Van Krevelen Diagram (Fig. S9). Molecules exhibiting a decrease in intensity have the most pronounced profile (Fig. 4). They represent 11 per cent of the whole molecules, and correspond to 24 per cent of the global intensity at 7 protons/MeOH, and decrease by a factor of 8 at 1500 photons/MeOH. Consequently, the major tendency is that the more the sample is irradiated, the less intense are the molecules. However, as previously noted, the diversity and the type of molecules are not impacted by a dose variation. Highly irradiation processes either form more ESI-invisible moieties (less oxygenated molecules) or are chemically less reactive.

Infrared spectroscopy analyses of the ice at low temperature (77 K) performed at the end of irradiation seem to be in favor of this second hypothesis. At this stage, CO_2 ($\nu(CO_2) = 2350\ cm^{-1}$) was quantified to estimate the amount of CH_3OH transformed in CO_2 (Fig. 5). A higher abundance of CO_2 is observed for higher photon doses. These differences cannot be only explained by an adsorption of CO_2 contamination because of the longer duration for experience at higher dose. This means that the variation of CO_2 is directly related to the number of photons received by CH_3OH and its photoproducts. Consequently, since more CH_3OH are transformed into CO_2, a non-reactive species for the formation of molecules forming residues, less methanol radicals such as HCO, CH_3O, or CH_2OH are available at high doses. This limits the quantity of molecules that are then formed during the warming phase. However, the dose is not sufficient to modify the chemistry and the type of radicals available before the warming phase. Indeed as observed, the structure of molecules is very similar whatever the dose is. This is probably due to the mode of formation of our ice, which is processed at the same time as its deposition. This means that new layers can be rapidly formed, diminishing the real photons per molecule. This would be different if a layer by layer experiment would be performed as observed for volatile organic compounds (Tenelanda-Osorio et al. 2022).

3.2. Impact on residue of the vacuum chamber pressure

In this section, the effect of an increase of the residual pressure inside the vacuum chamber on residue composition is investigated. Indeed, pressure variation can affect composition of residues depending on experimental conditions (Couturier-Tamburelli et al. 2023). In a classical experiment, the ice is warmed up with a dynamic pumping regime giving at 77 K an initial pressure of 10^{-7} mbars. To modify the residual pressure in the vacuum chamber, the latter was isolated from the turbomolecular pump with a trap. This gives at 77 K a residual pressure of 10^{-3} mbar. Then, the partial pressure was increased from 0 to 22 or to 216 mbars by adding argon into the chamber before starting the heating phase (see Table 1, PA, PB, PC, respectively). Initial ices were composed of H_2O: CH_3OH: NH_3 in the ratio 2:2:1 and irradiated during its formation with 33 photon/MeOH on average. The argon added in the chamber has a slight impact on the temperature increase of the ice (1.5–2.8 K min^{-1}), whereas the increase of the temperature at 10^{-7} mbar is around 2 K min^{-1}.

The modification of the pressure does not significantly modify the profile of infrared spectra whatever was the residual pressure considered. As seen in Fig. 2, only a slight decrease of infrared signatures and mass distribution intensities of residues are observed at higher pressure. However, molecular composition seems not to be impacted. As shown in Fig. 6, the group repartition is the same between the three experiments and the degree of aromaticity does not change significantly, except for the CHO group that presents a slightly higher aromaticity at low pressure. The pressure variation appears to have a greater impact on the yield of residue formed than on their molecular composition, but the overall impact is negligible.

3.3. Impact of heating rate on residue

During astrophysical ice experiments, once the ice is photoprocessed, the sample is heated up to 300 K. The temperature ramp was suggested to have an impact on the reactivity during this warming. Different heating rates at 0.5, 4, and 8.3 K min^{-1} (TA, TB, TC respectively, see Table 1) were tested using an ice composed at 77 K of H_2O: CH_3OH: NH_3 in ratio 3:1:1.5 with irradiation rates of 72, 87, or 214 photon/methanol. The residual pressure in the vacuum chamber during the warming was set as 10^{-7} mbars.

The whole intensity of the FT-IR spectrum is significantly lower at 0.5 K min^{-1}, which is confirmed by FT-ICR-MS measurement. The FT-IR data shows that the ester/acid band (band h in Fig. 2b) is clearly impacted as well as the one of –OH stretching (band b in Fig. 2b) suggesting that higher acidic compounds are formed at

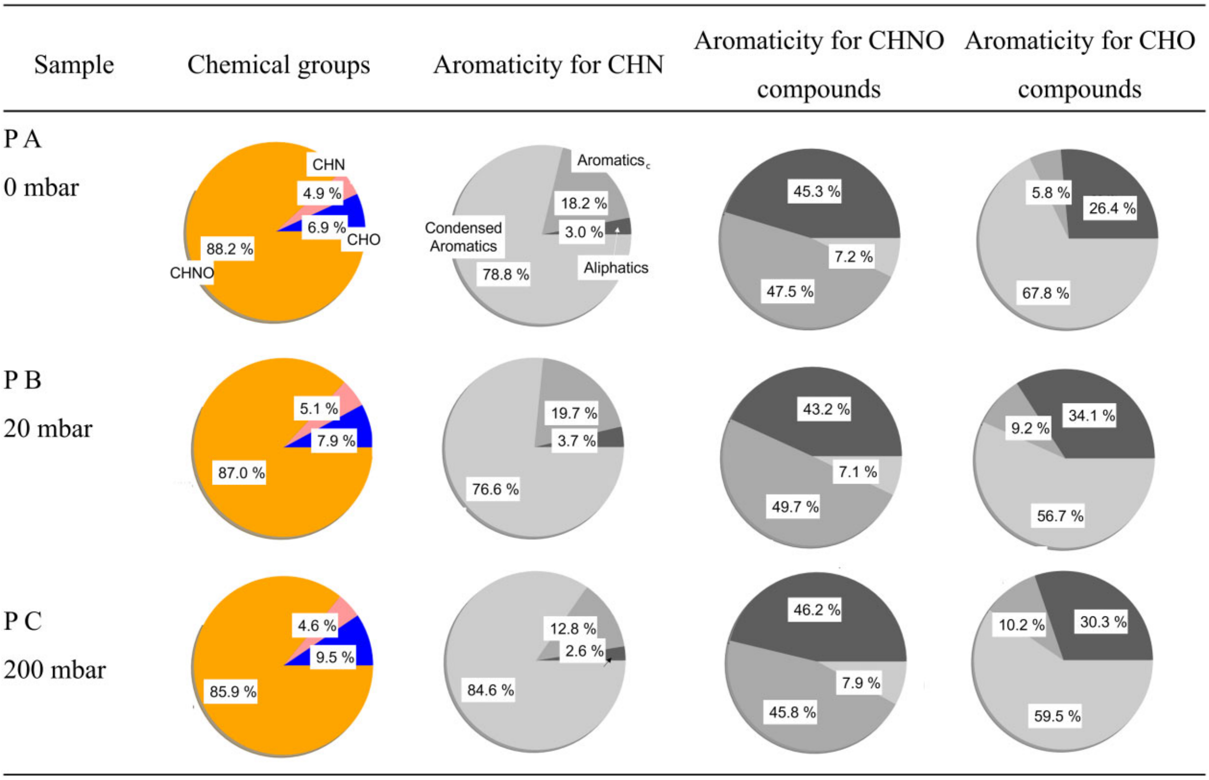

Figure 6. Proportions of attribution of ESI+ and ESI– combined data sets for the impact of the pressure. Pie charts are summarizing chemical groups, aliphaticities for CHN, CHNO, and CHO compounds. The aromaticity equivalent (χ_c) is defined in equation (2): a molecule is said to be aliphatic if $0 < \chi_c < 2.5$, aromatic if $2.5 < \chi_c < 2.7$ (benzene-type molecules) or condensed aromatic if $2.7 < \chi_c$ (PAH-type molecules). CHNO compounds are displayed in orange, CHN in pink, CHO in blue, aliphatic in dark grey, aromatics in grey, and condensed aromatics in light grey.

higher heating rates. Nevertheless, regarding FT-ICR data (Fig. 7), no significant alteration on the carbon structure of compounds is observed, except a weak increase of the aromaticity of the CHO group at 0.5 K min^{-1}, possibly confirming FT-IR observation on acid/ester bands evolution. Except for residue abundance, the heating rate does not seem to have an impact on residue composition.

4. ASTROPHYSICAL IMPLICATIONS

The formation of complex organic matter under irradiation is relevant to several astrophysical environments (Sandford et al. 2020; Rocha et al. 2023). Laboratory experiments involving irradiation of organics is an active field of research; and parameters we explored in this study can affect the relevance of experimental results to understand of the chemical reactivity in bodies of the Solar system (Öberg 2016).

Icy bodies within our Solar system are exposed to a variety of radiations, including UV photons from the Sun and energetic particles from the solar wind, cosmic rays, and magnetospheres (Islam et al. 2014, Ciaravella et al. 2020). Depending on their emplacement and history, the dose received varies considerably depending on the surface considered. Heating leading to the sublimation of the volatile phase, leaving only the refractory compounds, may have occurred over timescales impossible to replicate in an experiment (Mousis et al. 2016). Pressure conditions are also likely to vary considerably not only from body to body but also for a given body depending on diurnal, seasonal, and secular effects (Ciaravella et al. 2020).

The most direct applications of our experiment is the radiation processing of icy small bodies that later were included in the parent bodies of carbonaceous chondrites (CC); therefore, the abundant organic matter found in these meteorites (Alexander et al. 2017 and ref. therein) could be the result of radiation processing of ices (pre- and post-accretion), followed by sublimation as the parent body migrated to the inner Solar system. The parameters explored in this work (dose received, heating rates, and local pressure during sublimation) are all unconstrained for the history of CC parent bodies.

The same could be true of Ceres, for which an origin scenario has been proposed that involves formation in the remote regions of the Solar system, followed by migration into the asteroid belt ((De Sanctis et al. 2015). The outer layer of ice, previously exposed to UV/solar wind processing, would lose its volatiles during the migration, as water ice is unstable in the current conditions at Ceres' surface. The abundant organic matter detected on Ceres would then be the result of this process. As with CC parent bodies (see above), aqueous alteration is also very likely to be part of the history of the organic matter present today, as well as further irradiation of the organic matter. These phenomena are not considered in the present work but have been studied elsewhere (Danger et al. 2021; Serra et al. 2023; Garcia et al. 2024).

Another example relevant to our experiments is the proposed explanation for the reddening of Charon's poles. It has been modeled as the result of cyclic cold trapping of simple volatiles (including methane), along with their irradiation by solar wind and solar UV, forming complex organic matter (Grundy et al. 2016).

The surface of the icy moons around giant planets are also exposed to radiation processing, especially in the case of Jupiter (Cooper 2001; Paranicas et al. 2009), and any organic emplaced on the surface from the interior would be altered by energetic particle

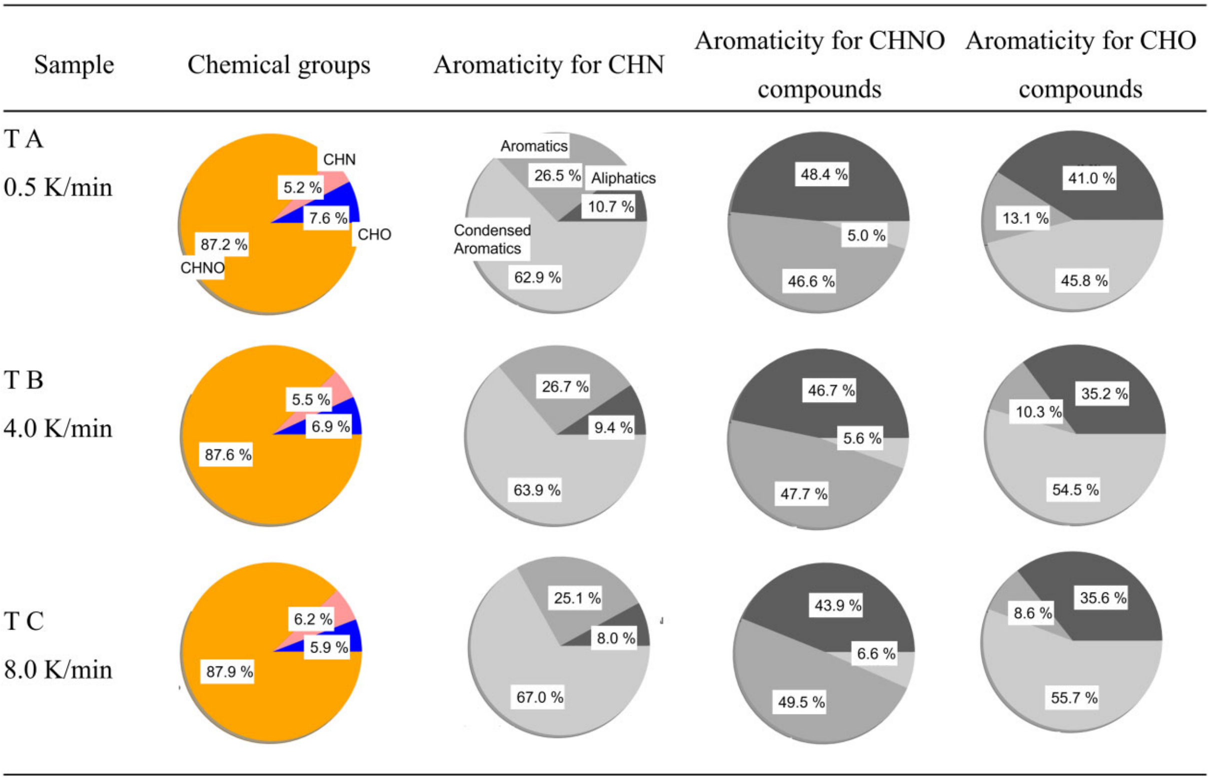

Figure 7. Proportions of attribution of ESI+ and ESI– combined data sets for the impact of the heating ramp. Pie charts are summarizing chemical groups and aliphaticities for CHN, CHNO, or CHO compounds. The aromaticity equivalent (χ_c) is defined equation 2: a molecule is said to be aliphatic if $0 < \chi_c < 2.5$, aromatic if $2.5 < \chi_c < 2.7$ (benzene-type molecules), or condensed aromatic if $2.7 < \chi_c$ (PAH-type molecules). CHNO compounds are displayed in orange, CHN in pink, CHO in blue, aliphatic in dark grey, aromatics in grey and condensed aromatics in light grey.

bombardment. While full devolatilization is unlikely to occur, some level of thermal processing is expected, as in the case of Europa, the extensive presence of crystalline water ice on the surface (Ligier et al. 2016) appears to indicate frequent heating events (Greenberg et al. 1998; O'Brien 2002).

Among the aforementioned examples, surface pressures are varied, but frequently estimated below the nanobar for icy dwarf planets and satellites (e.g. Stern et al. 2017) with phenomena like intense sputtering possibly increasing the exospheric density on some bodies (e.g. Vorburger et al. 2022).

The small impact of the parameters explored in this study means that irradiation experiments performed with the appropriate precursors provide relevant insights into the compositional evolution of organic matter in astrophysical bodies, even considering the uncertainties in heating rate or pressure. The causes for important compositional differences between laboratory results and astrophysical organic matter are more likely to be found in radiation dose, additional precursors, and/or additional processes, e.g. hydrothermal evolution (Vinogradoff et al. 2018; Danger et al. 2021).

In this study, only three parameters (photon dose, pressure, and heating rate during the warming process) were evaluated. As shown in other studies, other parameters can also modify the nature and abundance of residual photoproducts. For example, ices irradiated at low temperature show a higher diversity of photoproducts and residual products (Pilling et al., 2011, 2023b; Tenelanda-Osorio et al. 2022). Other irradiations sources were tested to irradiate astrophysical ices (electrons, X-rays, or ions), and showed differences in reactivities, leading to the formation of different compounds (Vasconcelos et al. 2017; Pilling et al. 2023b, 2023a).

5. CONCLUSION

In this study, we explored the experimental impact of heating rate, pressure of the vacuum chamber, and irradiation rate on the final composition of organic residues formed from H_2O: CH_3OH: NH_3 ices irradiated at Lyman α. Residue compositions were assessed by FT-IR and ESI-FT-ICR-MS for each condition. Identified organic compounds, mostly CHNO (76–86 per cent) contains up to 78 C, 188 H, 123 N, and 37 O.

The results obtained show the following:

(i) These three parameters (photon dose, pressure, and heating rate during the warming process) under our operating conditions have only a small impact on the molecular composition of the residue.

(ii) The pressure and the heating rate have only a weak impact on the abundance of the residue.

(iii) The irradiation rate is the most impacting parameter.

(iv) A high level of irradiation dose notably reduces the formation of the organic compounds forming the residue. We proposed that this is due to a higher formation of CO_2 at higher photon doses, this species being mainly unreactive in the formation of the carbon skeleton of the molecules of the residue.

ACKNOWLEDGEMENTS

The research was funded by the Centre National d'Etudes Spatiales (CNES, R-S18/SU-0003–072 and R-S18/SU-0003–072, PI: GD), and the Centre National de la Recherche Française (CNRS) with the programs 'Physique et Chimie du Milieu Interstellaire' (PCMI-PI: GD) and 'Programme National de Planétologie' (PNP) (PI: GD).

GD is grateful to the Agence Nationale de la Recherche for funding via the ANR RAHIIA_SSOM (ANR-16-CE29-0015) and VAHIIA (ANR-12-JS08-0001). The project has further received funding from the EXCellence Initiative of Aix-Marseille Université – A*Midex, a French 'Investissements d'Avenir programme' AMX-21-IET-018, from the Région SUD Provence Alpes Côte d'Azur 'Apog 2017' – PILSE, as well by the Deutsche Forschungsgemeinschaft (DFG, German Research Foundation) under Germany's Excellence Strategy – EXC 2094–390783311 (AR).

DATA AVAILABILITY STATEMENT

Data supporting the findings of this study are available from the corresponding author upon reasonable request. Interested researchers should contact the corresponding author for access to the data.

REFERENCES

Abou Mrad N., Duvernay F., Isnard R., Chiavassa T., Danger G., 2017, ApJ, 846, 124
Alexander C. M. O., Cody G. D., De Gregorio B. T., Nittler L. R., Stroud R. M., 2017, Geochemistry, 77, 227
Bernstein D. I., et al., 1995, ApJ, 454, 327
Bertaux J.-L., Lallement R., 2017, MNRAS, 469, S646
Bouilloud M., Fray N., Bénilan Y. et al., 2015, MNRAS, 451, 2145
Ciaravella A., Muñoz Caro G. M., Jiménez-Escobar A. et al., 2020, Proc. Natl. Acad. Sci. U.S.A., 117, 16149
Cooper J., 2001, Icarus, 149, 133
Couturier-Tamburelli I., Danger G., Mouzay J., Pardanaud C., Piétri N., 2023, J. Phys. Chem. A, 128, 636
Danger G. et al., 2013, Geochim. Cosmochim. Acta, 118, 184
Danger G. et al., 2016, Geochim. Cosmochim. Acta, 189, 184
Danger G. et al., 2022, A&A, 667, A120
Danger G. et al., 2021, Nat. Commun., 12, 1
De Sanctis M. C. et al., 2015, Nature, 528, 241
d'Hendecourt L., Dartois E., 2001, Spectrochim. Acta Part A, 57, 669
Fedoseev G., Cuppen H. M., Ioppolo S., Lamberts T., Linnartz H., 2015, MNRAS, 448, 1288
Fresneau A. et al., 2017, ApJ, 837, 168
Garcia A. et al., 2024, ACS Earth Space Chem., 8, 606
Gautier T. et al., 2020, Earth Planet. Sci. Lett., 531, 116011
Gioumouxouzis C. I., Kouskoura M. G., Markopoulou C. K., 2015, J. Chromatogr. B, 97, 998
Greenberg R. et al., 1998, Icarus, 135, 64
Grundy W. M. et al., 2016, Nature, 539, 65
Gutiérrez-Quintanilla A. et al., 2021, MNRAS, 506, 3734
Islam F., Baratta G. A., Palumbo M. E., 2014, 561, A73
Keller L. P., Thomas K. L., McKay D. S., 1994, AIP Conf. Proc., 310, 159
Layssac Y., Gutiérrez-Quintanilla A., Chiavassa T., Duvernay F., 2020, MNRAS, 496, 5292
Ligier N., Poulet F., Carter J., Brunetto R., Gourgeot F., 2016, AJ, 151, 163
Mousis O. et al., 2016, ApJ, 819, L33
Mumma M. J., Charnley S. B., 2011, Annu. Rev. Astron. Astrophys., 49, 471
Muñoz Caro G. M., Dartois E., Boduch P. et al., 2014, A&A, 566, A93
Muñoz Caro G. M., Schutte W. A., 2003, A&A, Vol. 412, 121
Nuevo M. et al., 2007, Adv. Space Res., 39, 400
Öberg K. I., 2016, Chem. Rev., 116, 9631
O'Brien D., 2002, Icarus, 156, 152
Oss M., Kruve A., Herodes K., Leito I., 2010, Anal. Chem., 82, 2865
Paranicas C., Cooper J. F., Garrett H. B., Johnson R. E., Sturner S. J., 2009, Europa, 529
Pilling S., da Silveira C. H., Ojeda-Gonzalez A., 2023, MNRAS, 523, 2858
Pilling S., Duarte E. S., Domaracka A., Rothard H., Boduch P., da Silveira E. F., 2011, Phys. Chem. Chem. Phys., 13, 15755
Pilling S., Rocha W. R. M., Carvalho G. A., de Abreu H. A., 2023, Adv. Space Res., 71, 5466
Pizzarello S., Shock E., 2010, Cold Spring Harb. Perspect. Biol., a002105, 1
Rocha W. R. M., Woitke P., Pilling S., Thi W.-F., Jørgensen J. K., Kristensen L.E., Perotti G., Kamp I., 2023, A&A, 673, A70
Ruf A., Bouquet A., Schmitt-Kopplin P., Boduch P., Mousis O., Danger G., 2021, A&A, 655, A74
Ruf A., Danger G., 2022, Anal. Chem. 94, 14135
Ruf A., Poinot P., Geffroy C., D'Hendecourt L. L. S., Danger G., 2019, Life, 9, 35
Sandford S. A., Nuevo M., Bera P. P., Lee T. J., 2020, Chem. Rev., 120, 4616
Schmitt-Kopplin P. et al., 2010, Proc. Natl. Acad. Sci. U.S.A., 107, 2763
Schutte W., Allamandola L., Sandford S., 1993, Icarus, 104, 118
Serra C., Vinogradoff V., Poinot P. et al. 2023, ACS Earth Sp Chem. 7, 1980
Stern S. A. et al., 2017, Icarus, 287, 124
Tenelanda-Osorio L. I. et al., 2022, MNRAS, 515, 5009
Tziotis D., Hertkorn N., Schmitt-Kopplin P., 2011, Eur J Mass Spectrom (Chichester), 17, 415
Vasconcelos F., de A., Pilling S., Rocha W. R. M., Rothard H., Boduch P., 2017, ApJ, 850, 174
Vinogradoff V., Bernard S., Le Guillou C., Remusat L., 2018, Icarus, 305, 358
Vinogradoff V., Rimola A., Duvernay F., Danger G., Teulé P., Chiavassa P., 2012, Phys. Chem. Chem. Phys., 14, 12309
Vorburger A., Fatemi S., Galli A., Luizzo L., Pope A.R., Wurz P., 2022, Icarus, 375, 114810
Wooden D. H., Charnley S. B., Ehrenfreund P., 2004, Comets, II, 33
Yassine M. M., Harir M., Dabek-Zlotorzynska E., Schmitt-Kopplin P., 2014, Rapid Comm Mass Spectrometry, 28, 2445

SUPPORTING INFORMATION

Supplementary data are available at *MNRAS* online.

This paper has been typeset from a TEX/LATEX file prepared by the author.